Experimental model updating using frequency response functions

Yu Hong[a, b], Xi Liu[b], Xinjun Dong[b], Yang Wang*[b], Qianhui Pu[a]
[a] School of Civil Eng., Southwest Jiaotong University, Chengdu, Sichuan 610031, China
[b] School of Civil and Environmental Eng., Georgia Inst. of Technology, Atlanta, GA 30332, USA

ABSTRACT

In order to obtain a finite element (FE) model that can more accurately describe structural behaviors, experimental data measured from the actual structure can be used to update the FE model. The process is known as FE model updating. In this paper, a frequency response function (FRF)-based model updating approach is presented. The approach attempts to minimize the difference between analytical and experimental FRFs, while the experimental FRFs are calculated using simultaneously measured dynamic excitation and corresponding structural responses. In this study, the FRF-based model updating method is validated through laboratory experiments on a four-story shear-frame structure. To obtain the experimental FRFs, shake table tests and impact hammer tests are performed. The FRF-based model updating method is shown to successfully update the stiffness, mass and damping parameters of the four-story structure, so that the analytical and experimental FRFs match well with each other.

Keywords: frequency response function, finite element model updating, shake table test, hammer test

1. INTRODUCTION

Although significant improvements have been made in FE modeling during the past few decades, it remains challenging to obtain an FE model that can fully represent an actual structure in the field. The inaccuracies in FE models can possibly be caused by nominal material property values, improper boundary conditions, difficulties in damping modeling, etc. Therefore, to achieve higher simulation accuracy, an initial FE model built according to design drawings needs to be updated using field experimental data.

Over the past few decades, many FE model updating methods have been proposed and practically applied [1]. These methods can be broadly classified into two categories: modal-based methods and response-based methods. Modal-based model updating methods need to extract modal properties (such as resonance frequencies, mode shapes and damping ratios) from experimental data first. These modal properties are then utilized to update the FE model. For example, modal property difference approach belongs to the modal-based category. The approach updates model parameter values by minimizing the discrepancies between the simulated and experimental modal properties. Brownjohn and Xia proposed a method to perform model updating by minimizing the frequency difference between experiments and simulation [2]. Teughels *et al*. extended this method to minimize both mode shape difference and frequency difference and applied the new method on a railway bridge [3]. Jaishi and Ren proposed an objective function which contains frequency residual, modal assurance criterion (MAC) related function, and modal flexibility residual for model updating [4]. Another representative in modal-based category is called modal dynamic residual approach, which attempts to update the mass, stiffness and damping information by minimizing the modal dynamic residuals from the generalized eigenvalue equation. For example, Abdalla *et al*. proposed an optimization problem involving modal dynamic residual constraints on the unknown stiffness matrix [5]. Zhu *et al*. compared the modal property difference approach and dynamic residual approach on a lumped mass-spring model [6]. However, all these modal-based methods need to first perform modal analysis to experimental data. This may add uncertainties and errors during the model updating process. Another difficulty is that, in most cases, only the first few natural frequencies and mode shapes of a structure can be extracted through modal analysis. As a result, the modal property data available for model updating are limited.

In the response-based category, vibration response time history-based method is one representative. Agbabian *et al.* first proposed to use vibration time history data for structural damage detection of a 3-DOF numerical model [7]. Cattarius and Inman utilized the beat phenomena to find changes in vibration response to detect the damage of a cantilevered aluminum

*yang.wang@ce.gatech.edu; phone +1 404 894-1851; http://wang.ce.gatech.edu

Sensors and Smart Structures Technologies for Civil, Mechanical, and Aerospace Systems 2016,
edited by Jerome P. Lynch, Proc. of SPIE Vol. 9803, 980325 · © 2016 SPIE
CCC code: 0277-786X/16/$18 · doi: 10.1117/12.2219364

plate [8]. Although time domain methods have a lot of advantages, they require significant computational efforts. Another representative in response-based category is the FRF-based model updating method. The FRF-based method requires to use experimental FRFs, which can be easily calculated through structural response data and excitation data. Thus, the FRF-based method provides the convenience of not requiring the extraction of modal properties. In addition, an experiment can provide abundant data in a large frequency range, as opposed to modal information which is limited to only a few identified frequencies and modes.

Among FRF-based approaches, Lin and Ewins presented an analytical sensitivity-based FRF updating method, which avoids the inverse of the system dynamic stiffness matrix [9]. Later, Lin and Zhu extended this method to update the general damped structural model [10]. According to Lin and Ewins' work, Arora *et al*. proposed a two-step procedure to update the mass and stiffness matrices first, and then identify damping [11]. Pradhan and Modak modified the sensitivity-based FRF method by only using the real-valued normal FRF matrix (for a corresponding undamped system) in the model updating [12]. Nevertheless, this analytical sensitivity-based FRF method has a main drawback of requiring complete measurements at all DOFs. This is unrealistic in practice, so expansion of the measured FRF or reduction of system matrices is required, which will add inaccuracies to the model updating process. To overcome this limitation, Sipple and Sanayei proposed a numerical sensitivity-based FRF method which uses the modal-decomposed form of analytical FRF in FE model updating [13]. The proposed expression of FRF is in scalar form, so this method does not need any expansion of the experiment FRF data or reduction of system matrices.

This research follows the numerical sensitivity-based FRF method that attempts to minimize the difference between analytical and experimental FRFs [13]. In comparison with the previous work that's equivalent to Caughey damping assumption, the FRF formulation for a simpler Rayleigh damping assumption is provided here. In addition, besides the default scenario where excitation is applied at only one degree-of-freedom (DOF) at a time, the FRF formulation is derived for the scenario where ground/earthquake excitation occurs to a shear-frame building structure (which is equivalent to applying excitation simultaneously at all DOFs). To validate these formulations towards FRF-based model updating, laboratory experiments are performed on a four-story aluminum structure. The rest of the paper is organized as follows. Section 2 presents the formulations of FRFs with Rayleigh and Caughey damping assumptions, for both of the excitation scenarios. Section 3 describes the model updating process that minimizes the difference between analytical and experimental FRFs. Section 4 describes the hammer tests and shake table test on a four-story shear-frame aluminum structure for validating the performances of the proposed formulations for FRF-based model updating. Finally, conclusions and future work are provided in section 5.

2. FORMULATIONS OF THE FREQUENCY RESPONSE FUNCTION

2.1 Analytical form of the frequency response function for excitation at one DOF

The presented formulations for one-DOF excitation is based on the derivation in Sipple and Sanayei's work, which avoids the use of analytical sensitivity [13]. The FRF for single-DOF excitation can be experimentally obtained using excitations like hammer impact. Analytical natural frequency, mode shape, and damping ratio for every mode are needed for the updating, which can be easily obtained from the FE model.

The derivation begins from the basic form of the frequency response function. For an *n*-DOF structure with viscous damping, the FRF for displacement can be written as:

$$\mathbf{H}(\omega) = \left(-\omega^2\mathbf{M} + \mathbf{K} + \mathrm{j}\omega\mathbf{C}\right)^{-1} \tag{1}$$

The FRF in Eq. (1) is defined as receptance. Here $\mathbf{M} \in \mathbb{R}^{n\times n}$ is the mass matrix; $\mathbf{K} \in \mathbb{R}^{n\times n}$ is the stiffness matrix; $\mathbf{C} \in \mathbb{R}^{n\times n}$ is the damping matrix; $\mathrm{j} = \sqrt{-1}$ is the imaginary unit; ω is a (angular) frequency point.

When assuming proportional damping, the damped system has real-valued modes as the corresponding undamped system. Rayleigh damping model is one of the most widely used proportional damping model.

$$\mathbf{C} = a_0\mathbf{M} + a_1\mathbf{K} \tag{2}$$

where a_0 is the damping coefficient related to mass matrix and a_1 is the damping coefficient related to stiffness matrix.

Substituting Eq. (2) into Eq. (1), we get

$$\mathbf{H}(\omega)=\left[\left(-\omega^2+\mathrm{j}a_0\omega\right)\mathbf{M}+\left(1+\mathrm{j}a_1\omega\right)\mathbf{K}\right]^{-1} \tag{3}$$

Then take the inverse of both sides of Eq. (3) and pre-multiply and post-multiply both sides by $\mathbf{\Phi}^{\mathrm{T}}$ and $\mathbf{\Phi}$, respectively, where $\mathbf{\Phi}$ is the mass-normalized mode shape matrix, i.e., $\mathbf{\Phi}^{\mathrm{T}}\mathbf{M}\mathbf{\Phi}=\mathbf{I}$, $\mathbf{\Phi}^{\mathrm{T}}\mathbf{K}\mathbf{\Phi}=\mathbf{\Omega}^2$.

$$\mathbf{\Phi}^{\mathrm{T}}\mathbf{H}(\omega)^{-1}\mathbf{\Phi}=\mathbf{\Phi}^{\mathrm{T}}\left[\left(-\omega^2+\mathrm{j}a_0\omega\right)\mathbf{M}+\left(1+\mathrm{j}a_1\omega\right)\mathbf{K}\right]\mathbf{\Phi} \tag{4}$$

where $\mathbf{\Omega}$ is a diagonal matrix containing the undamped natural frequencies.

After simplifying the equation, using modal orthogonality, Eq.(4) can be written as:

$$\mathbf{\Phi}^{\mathrm{T}}\mathbf{H}(\omega)^{-1}\mathbf{\Phi}=\left(-\omega^2+\mathrm{j}a_0\omega\right)\mathbf{I}+\left(1+\mathrm{j}a_1\omega\right)\mathbf{\Omega}^2 \tag{5}$$

In order to eliminate the inverse of $\mathbf{H}(\omega)$, first pre-multiply each side of the equation by $\mathbf{\Phi}^{-\mathrm{T}}$ and post-multiply each side by $\mathbf{\Phi}^{-1}$, and then take the inverse of Eq. (5):

$$\mathbf{H}(\omega)=\mathbf{\Phi}\left[\left(-\omega^2+\mathrm{j}a_0\omega\right)\mathbf{I}+\left(1+\mathrm{j}a_1\omega\right)\mathbf{\Omega}^2\right]\mathbf{\Phi}^{\mathrm{T}} \tag{6}$$

Further decompose Eq.(6) into the summation of mode shapes at every DOF:

$$H_{r,e}(\omega)=\sum_{i=1}^{m}\frac{\phi_{r,i}\phi_{e,i}}{-\omega^2+{\omega_{n,i}}^2+\mathrm{j}\left(a_0+a_1{\omega_{n,i}}^2\right)\omega} \tag{7}$$

In Eq.(7), *m* is the total number of modes; the subscripts *r* and *e* represent the response DOF and excitation DOF, respectively; $\phi_{r,i}$ and $\phi_{e,i}$ are the *r*-th and *e*-th entry of the *i*-th mass-normalized mode shape vector $\boldsymbol{\varphi}_i$, respectively; $\omega_{n,i}$ is the undamped natural frequency for *i*-th mode.

As a general from of proportional damping, Caughey damping model is also utilized here for deriving the FRF. Caughey damping is expressed as a series expression relate to mass and stiffness matrices [14].

$$\mathbf{C}=\mathbf{M}\sum_{l=0}^{m-1}a_l\left[\mathbf{M}^{-1}\mathbf{K}\right]^l \tag{8}$$

where $a_l\,(l=0,...,m-1)$ are constants associated with mass and stiffness matrices. The damping ratio for the *i*-th mode is thus:

$$\xi_i=\frac{1}{2}\sum_{l=0}^{m-1}a_l\,\omega_{n,i}^{2l-1} \tag{9}$$

Following the previous derivation, it is easy to get the modal-decomposed form of FRF for Caughey damping assumption.

$$H_{r,e}(\omega)=\sum_{i=1}^{m}\frac{\phi_{r,i}\phi_{e,i}}{-\omega^2+2\mathrm{j}\xi_i\omega_{n,i}\omega+\omega_{n,i}^2} \tag{10}$$

Besides the (displacement) receptance FRF $H_{r,e}(\omega)$, mobility $Y_{r,e}(\omega)$ is defined as the FRF for excitation at DOF-*e* and the corresponding velocity response at DOF-*r*. Accelerance $A_{r,e}(\omega)$ is defined as the FRF for the excitation at DOF-*e* and the corresponding acceleration response at DOF-*r*. Both the mobility function and the accelerance function can be easily calculated from the receptance function.

$$Y_{r,e}(\omega)=\mathrm{j}\omega H_{r,e}(\omega) \tag{11}$$

$$A_{r,e}(\omega)=-\omega^2 H_{r,e}(\omega) \tag{12}$$

2.2 Analytical form of the frequency response function for ground excitation

The experimental study in this research includes ground/earthquake excitation to a 4-story laboratory structure. The analytical form of the FRF with ground excitation is extended from the previous one-DOF excitation case. For an *n*-DOF shear-frame structure, the response at DOF-*r* caused by ground acceleration can be taken as the summation of responses at DOF-*r* caused by the equivalent earthquake force at every DOF [15]. $X_{r,e}(\omega)$ represents displacement response at DOF-*r* due to the excitation at DOF-*e* in frequency domain, m_e is the lumped mass at DOF-*e*.

$$X_r(\omega) = \sum_{e=1}^{n} X_{r,e}(\omega) = \sum_{e=1}^{n} H_{r,e}(\omega) F_e(\omega) = \sum_{e=1}^{n} -H_{r,e}(\omega) A_{\text{ground}}(\omega) m_e \tag{13}$$

The receptance for response at location *r* due to ground excitation can be derive from Eq. (13):

$$H_{r,\text{ground}}(\omega) = \frac{X_r(\omega)}{A_{\text{ground}}(\omega)} = \sum_{e=1}^{n} -H_{r,e}(\omega) m_e \tag{14}$$

For Rayleigh damping case, the analytical form of receptance for ground acceleration can be written as:

$$H_{r,\text{ground}}(\omega) = \sum_{i=1}^{m} \frac{-\phi_{r,i} \sum_{e=1}^{n} m_e \phi_{e,i}}{-\omega^2 + \omega_{n,i}^2 + \text{j}\left(a_0 + a_1 \omega_{n,i}^2\right)\omega} \tag{15}$$

For Caughey damping case, the analytical form of receptance for ground acceleration can be written as:

$$H_{r,\text{ground}}(\omega) = \sum_{i=1}^{m} \frac{-\phi_{r,i} \sum_{e=1}^{n} m_e \phi_{e,i}}{-\omega^2 + 2\text{j}\xi_i \omega_{n,i} \omega + \omega_{n,i}^2} \tag{16}$$

3. FREQUENCY RESPONSE FUNCTION-BASED MODEL UPDATING METHOD

3.1 Frequency response function form used in model updating method

From the FRF formulations in Eq. (7), (10), (15), (16), it is easy to find that the FRF value for any damped system is a complex number. In the model updating process, the magnitude of FRF, $\overline{H}_{r,e}(\omega)$ and $\overline{H}_{r,\text{ground}}(\omega)$ are often recommended for adoption [13].

$$\begin{aligned} \overline{H}_{r,e}(\omega) &= \left| H_{r,e}(\omega) \right| \\ \overline{H}_{r,\text{ground}}(\omega) &= \left| H_{r,\text{ground}}(\omega) \right| \end{aligned} \tag{17}$$

The magnitude of each DOF value is one scalar. Whenever practically possible, it is preferred to obtain FRFs from multiple response DOFs, due to multiple excitation DOFs, and at a great number of interested frequency points. In order to use all these FRF data for model updating, long vectors are formulated.

For one-DOF excitation,

$$\mathbf{H} = \left\{ \left[\overline{\mathbf{H}}_{r_a,e_b}^{\text{T}}(\omega_1), \cdots, \overline{\mathbf{H}}_{r_a,e_b}^{\text{T}}(\omega_{n_\omega}) \right], \cdots, \left[\overline{\mathbf{H}}_{r_p,e_q}^{\text{T}}(\omega_1), \cdots, \overline{\mathbf{H}}_{r_p,e_q}^{\text{T}}(\omega_{n_\omega}) \right] \right\}^{\text{T}} \tag{18}$$

For ground excitation,

$$\mathbf{H} = \left\{ \left[\overline{\mathbf{H}}_{r_a,\text{ground}}^{\text{T}}(\omega_1), \cdots, \overline{\mathbf{H}}_{r_a,\text{ground}}^{\text{T}}(\omega_{n_\omega}) \right], \cdots, \left[\overline{\mathbf{H}}_{r_p,\text{ground}}^{\text{T}}(\omega_1), \cdots, \overline{\mathbf{H}}_{r_p,\text{ground}}^{\text{T}}(\omega_{n_\omega}) \right] \right\}^{\text{T}} \tag{19}$$

The subscripts r_a, r_p represent different response DOFs and e_b, e_q represent different excitation DOFs. The excitation-response index pairs should include all scenarios for which experimental testing data is available. In addition, ω_i (i =1,…,

n_ω) is a frequency point, an n_ω is the total number of available frequency points. The selected frequency points can affect the updating results, so these points need to be carefully chosen based on experimental FRF plots. The selected regions of FRF data cannot be susceptible to sensor noise. Half-power bandwidth is recommended in this paper to choose the frequency points around every peak in the FRF plot, which corresponds to every obvious resonance frequency in the plot.

The model updating approach in this paper attempts to minimize the difference between analytical and experimental FRFs. We use $\mathbf{H}^{\mathrm{E}}$ to denote the long experimental FRF vector, and $\mathbf{H}^{\mathrm{A}}$ for the analytical counterpart.

3.2 Optimization problems for model updating

For a linear structural system, the updating variables associated with the stiffness and mass information can be updated as Eq. (20) and Eq. (21) , respectively.

$$\mathbf{K} = \mathbf{K}_0 + \sum_{r=1}^{n_\alpha} \alpha_r \mathbf{K}_{0,r} \tag{20}$$

$$\mathbf{M} = \mathbf{M}_0 + \sum_{r=1}^{n_\beta} \beta_r \mathbf{M}_{0,r} \tag{21}$$

where $\mathbf{K}_0$ and $\mathbf{M}_0$ are the constant initial stiffness and mass matrices from original FE model; n_α and n_β represent the total number of corresponding updating variables; α_r and β_r are the scalar multipliers associated with physical parameters to be updated, such as Young's modulus, mass density, support spring stiffness, etc; $\mathbf{K}_{0,r}$ and $\mathbf{M}_{0,r}$ are the constant influence matrices that corresponded to α_r and β_r, respectively. The updating variables associated with damping can be damping coefficients a_0 and a_1 for Rayleigh damping model (Eq. (2)), and damping ratios ξ_i (i = 1,…, m) for Caughey damping model (Eq. (8)).

The objective function for the FRF-based FE model updating shows the difference between the experimental FRF and analytical FRF. In order to obtain the optimal value for those updating variables, objective function value needs to be minimized under constraints. For Rayleigh damping case with one-DOF excitation, objective function in Eq. (22a) is used.

$$\underset{\boldsymbol{\alpha},\boldsymbol{\beta},a_0,a_1}{\text{minimize}} \left\| \mathbf{H}^{\mathrm{A}}\left(\boldsymbol{\alpha},\boldsymbol{\beta},a_0,a_1\right) - \mathbf{H}^{\mathrm{E}} \right\|^2 \tag{22a}$$

$$\text{subject to } \left[\mathbf{K}\left(\boldsymbol{\alpha}\right) - \omega_{\mathrm{n},i}^2 \mathbf{M}\left(\boldsymbol{\beta}\right)\right]\boldsymbol{\varphi}_i = \mathbf{0} \tag{22b}$$

$$\mathbf{H} = \left\{ \left[\overline{\mathbf{H}}_{r_a,e_b}^{\mathrm{T}}(\omega_1), \cdots, \overline{\mathbf{H}}_{r_a,e_b}^{\mathrm{T}}(\omega_{n_\omega}) \right], \cdots, \left[\overline{\mathbf{H}}_{r_p,e_q}^{\mathrm{T}}(\omega_1), \cdots, \overline{\mathbf{H}}_{r_p,e_q}^{\mathrm{T}}(\omega_{n_\omega}) \right] \right\}^{\mathrm{T}} \tag{22c}$$

$$H_{r,e}(\omega) = \sum_{i=1}^{m} \frac{\phi_{r,i}\phi_{e,i}}{-\omega^2 + {\omega_{n,i}}^2 + \mathrm{j}\left(a_0 + a_1 {\omega_{n,i}}^2\right)\omega} \tag{22d}$$

$$\boldsymbol{\alpha}^l \le \boldsymbol{\alpha} \le \boldsymbol{\alpha}^u; \quad \boldsymbol{\beta}^l \le \boldsymbol{\beta} \le \boldsymbol{\beta}^u \tag{22e}$$

$$a_0{}^l \le a_0 \le a_0{}^u; \; a_1{}^l \le a_1 \le a_1{}^u \tag{22f}$$

where $\|\cdot\|$ denotes any norm function; $\boldsymbol{\alpha}$, $\boldsymbol{\beta}$, a_0, a_1 are the selected updating variables. Updated variables are subjected to constraints with lower bound and upper bound. Superscripts l and u denote the lower bound and upper bound of the corresponding updating variable, respectively; m is the total number of analytical modes used in model updating.

For Rayleigh damping case with ground excitation, Eq. (22c) in the optimization problem is to be replaced by the following, and Eq. (22d) should be replaced by Eq. (15) accordingly.

$$\mathbf{H} = \left\{ \left[\overline{\mathbf{H}}_{r_a,\mathrm{ground}}^{\mathrm{T}}(\omega_1), \cdots, \overline{\mathbf{H}}_{r_a,\mathrm{ground}}^{\mathrm{T}}(\omega_{n_\omega}) \right], \cdots, \left[\overline{\mathbf{H}}_{r_p,\mathrm{ground}}^{\mathrm{T}}(\omega_1), \cdots, \overline{\mathbf{H}}_{r_p,\mathrm{ground}}^{\mathrm{T}}(\omega_{n_\omega}) \right] \right\}^{\mathrm{T}} \tag{23}$$

For Caughey damping case with one-DOF excitation, objective function in Eq. (24a) and the transfer function matrix in Eq. (10) should be used. The complete optimization problem is provided as follows.

$$\underset{\boldsymbol{\alpha},\boldsymbol{\beta},\boldsymbol{\xi}}{\text{minimize}} \left\| \mathbf{H}^{\mathrm{A}}\left(\boldsymbol{\alpha},\boldsymbol{\beta},\boldsymbol{\xi}\right) - \mathbf{H}^{\mathrm{E}} \right\|^2 \tag{24a}$$

$$\text{subject to } \left[\mathbf{K}\left(\boldsymbol{\alpha}\right) - \omega_{n,i}^2 \mathbf{M}\left(\boldsymbol{\beta}\right)\right]\boldsymbol{\varphi}_i = \mathbf{0} \tag{24b}$$

$$\mathbf{H} = \left\{\left[\overline{\mathbf{H}}_{r_a,e_b}^{\mathrm{T}}(\omega_1),\cdots,\overline{\mathbf{H}}_{r_a,e_b}^{\mathrm{T}}(\omega_{n_\omega})\right],\cdots,\left[\overline{\mathbf{H}}_{r_p,e_q}^{\mathrm{T}}(\omega_1),\cdots,\overline{\mathbf{H}}_{r_p,e_q}^{\mathrm{T}}(\omega_{n_\omega})\right]\right\}^{\mathrm{T}} \tag{24c}$$

$$H_{r,e}(\omega) = \sum_{i=1}^{m} \frac{\phi_{r,i}\,\phi_{e,i}}{-\omega^2 + 2\mathrm{j}\xi_i\omega_{n,i}\omega + \omega_{n,i}^2} \tag{24d}$$

$$\boldsymbol{\alpha}^l \le \boldsymbol{\alpha} \le \boldsymbol{\alpha}^u;\quad \boldsymbol{\beta}^l \le \boldsymbol{\beta} \le \boldsymbol{\beta}^u \tag{24e}$$

$$\boldsymbol{\xi}^l \le \boldsymbol{\xi} \le \boldsymbol{\xi}^u \tag{24f}$$

where $\boldsymbol{\xi} = \left[\xi_1,...,\xi_m\right]^{\mathrm{T}}$ are the selected damping updating variables.

Similarly, for Caughey damping case with ground excitation, the transfer function vector Eq. (24c) in the optimization problem is to be replaced by Eq. (23), and the transfer function (24d) is to be replaced by Eq. (16). A global optimization toolbox, 'Multistart', together with a nonlinear least square optimization solver, 'lsqnonlin' in MATLAB toolbox (Math Works Inc., 2005), are adopted to find the optimal solution of the optimization problems above.

4. EXPERIMENTAL VALIDATION

To validate the FRF-based model updating method described in Section 3, a four-story shear-frame laboratory structure is built. In the first test scenario, hammer excitation is applied at every floor of the structure. In the second test scenario, shake table is used to generate ground excitation.

4.1 Testbed structure

Figure 1 shows the test structure mounted on a shake table. All the columns and the floors are made of aluminum alloy. The weight of every floor is 4.64kg (10.24 lbs.). Every story has 8 thin columns, which have the same rectangular section of: 0.0254m × 0.00159m (1 in. × 1/16 in.). The nominal Young's modulus value of the aluminum columns is 63GPa. The total height of the building is 1.182m (46.5 in.). The first three stories have the same height: 0.305m (12 in.), while the fourth story is 0.267m (10.5 in.). Fixed connections are applied at the end of the every column. Every floor can be taken as a rigid mass, and the columns mainly provide the lateral stiffness of the structure. Therefore, this four-story shear-frame structure can be idealized as a 4-DOF system.

Every floor is instrumented with an accelerometer (Crossbow CXL01LF1) and a displacement sensor (Temposonics CS194AV) for measuring lateral vibration. Both sensors are interfaced with a wireless sensing system, *Martlet* [16]. Because kilo-Hertz high frequency sampling is needed for the impact hammer, an additional cabled National Instruments data acquisition system is used. A reference accelerometer (Crossbow CXL01LF1) is added on the fourth floor (show in Figure 1), and sampled by the cabled system. With one wireless accelerometer and one cabled accelerometer on the same floor, data from the two systems can be synchronized.

4.2 Hammer test

Before hammer tests, base fixtures are installed to hold the ground/base plate still during the test. The sampling frequency of the wireless sensing system is set to be 500Hz, and the sampling frequency for the cabled system with the impact hammer (Brüel & Kjær 8206-001) is set as 5000Hz. Figure 2 shows data from an example hammer impact at the 1st floor. After data synchronization, the 4th floor accelerations from the cabled system and wireless system can match well (Figure 3).

In order to obtain more FRF data, a hammer impact is applied to every floor. After obtaining all the displacement and acceleration responses, the receptances and accelerances for hammer tests are calculated. In this paper, only the four peak areas of the FRF curves are used for model updating. Table 1 summarizes updating results from hammer tests. Receptances and accelerances considering Rayleigh damping model and Caughey damping model are used, respectively. The initial

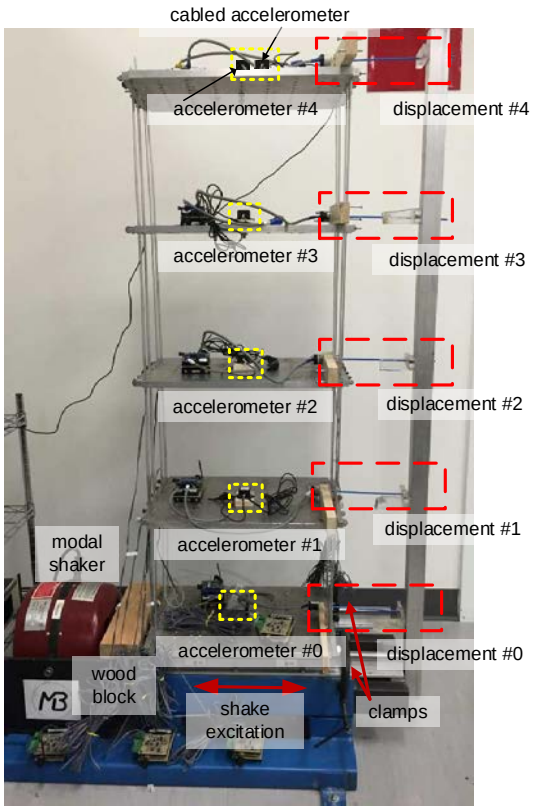

Figure 1. The test structure and experimental setup

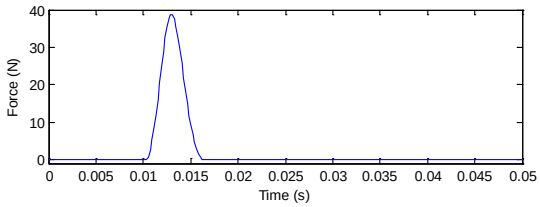

Figure 2. Example hammer impact applied at the 1st floor

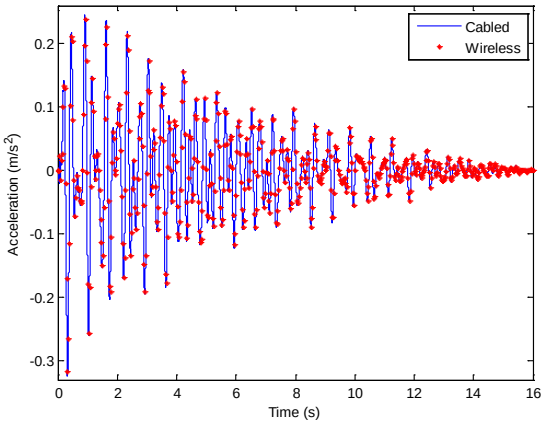

Figure 3. Data synchronization between cabled and wireless sensing system

mass value for every floor only includes the contribution of plate mass. The inter-story stiffness is mainly contributed by the fixed-end shear stiffness from columns. The initial story stiffness values are calculated based on the nominal aluminum Young's modulus, while considering the relatively significant P-Δ effect. Since damping information is least known, the initial values are chosen based on experience. In addition, during the updating process, the lower bounds and upper bounds for damping variables are set to be large. In the last column of Table 1, the relative standard deviation (RSD) for every variable is used to evaluate how well the model updating results obtained from different types of responses with different damping models agree with each other. The RSD is expressed in percentage. A small number means good agreement, while a large number means great dispersion. In this test, the largest RSD value of the updating variable is only 1.322%. Since Rayleigh damping and Caughey damping have different parameters in the model updating process, Table 1 does not calculate RSD value for damping information. For Rayleigh damping model, since a_0 is much larger than a_1, the damping contribution from a_1 can be neglected. This type of damping can be considered as mass-proportional damping. For Caughey damping model, it is easy to observe that the updating result of damping ratio for every mode is consistent between the receptance and accelerance-based approaches.

Figure 4 shows the updated FRF plots using Rayleigh damping model. Figure 4 (a) compares the initial, the experimental and the updated receptance $\mathbf{H}_{4,1}$. Figure 4 (b) shows the comparison for accelerance $\mathbf{A}_{4,1}$. The peak areas for these updated FRF curves can match well with the peak areas of experimental FRF curves. The frequency domain assurance criterion (FDAC) [17] value is utilized to compare the similarity between the peak areas of the updated and experimental FRFs. A value 1 means perfect correlation, 0 means no correlation at all. The FDAC value in Figure 4 (a) is 0.955 and the FDAC value in Figure 4 (b) is 0.971.

Table 1. Model updating results from impact hammer tests

Parameter		Initial	Rayleigh damping		Caughey damping		RSD (%)
			Updated (Receptance)	Updated (Accelerance)	Updated (Receptance)	Updated (Accelerance)	
Mass (kg)	m_1	4.64	5.155	5.155	5.155	5.155	0.001
	m_2	4.64	4.953	4.953	5.030	4.977	0.733
	m_3	4.64	4.949	4.949	4.949	4.949	0.000
	m_4	4.64	5.090	5.143	5.105	5.143	0.524
Stiffness (N/m)	k_1	1019	1089.677	1073.751	1097.386	1108.075	1.322
	k_2	1217	1257.784	1261.664	1270.792	1259.538	0.458
	k_3	1420	1378.311	1395.234	1382.871	1364.084	0.932
	k_4	2473	2665.588	2659.859	2670.688	2688.651	0.466
Damping	a_0 or ξ_1	0.01 / 0.01	0.2210	0.2670	0.0168	0.0163	-
	a_1 or ξ_2	10^{-6} / 0.01	10^{-10}	10^{-10}	0.0115	0.0114	-
	ξ_3	0.01	-	-	0.0051	0.0049	-
	ξ_4	0.01	-	-	0.0021	0.0020	-

Figure 5 shows the updated FRF plots using Caughey damping model. Figure 5 (a) compares the initial, the experimental and the updated receptance $\mathbf{H}_{3,4}$. Figure 5 (b) shows the comparison for accelerance $\mathbf{A}_{3,4}$. The peak areas for these updated FRF curves can match well with the peak areas of experimental FRF curves. The FDAC value in Figure 5 (a) is 0.987 and the FDAC value in Figure 5 (b) is 0.975. Overall, FDAC values in Caughey damping case are larger than those in Rayleigh damping case, since Caughey damping has more updating variables. The size of the structure used in this model updating is small, so the computation time difference is negligible for the model updating processes with these two damping models. However, FE model updating for a large structure with Caughey damping model may cost more time than Rayleigh damping model.

4.3 Shake table (ground excitation) test

In order to validate model updating using ground excitation formulations, in Eq.(15) and Eq.(16), a shake table test is conducted. The modal shaker is able to generate horizontal base acceleration to the structure, as shown in Figure 1. During the shaker test, the fixtures are removed from the ground floor. A chirp signal ranging from 0Hz to 10Hz within 60s is

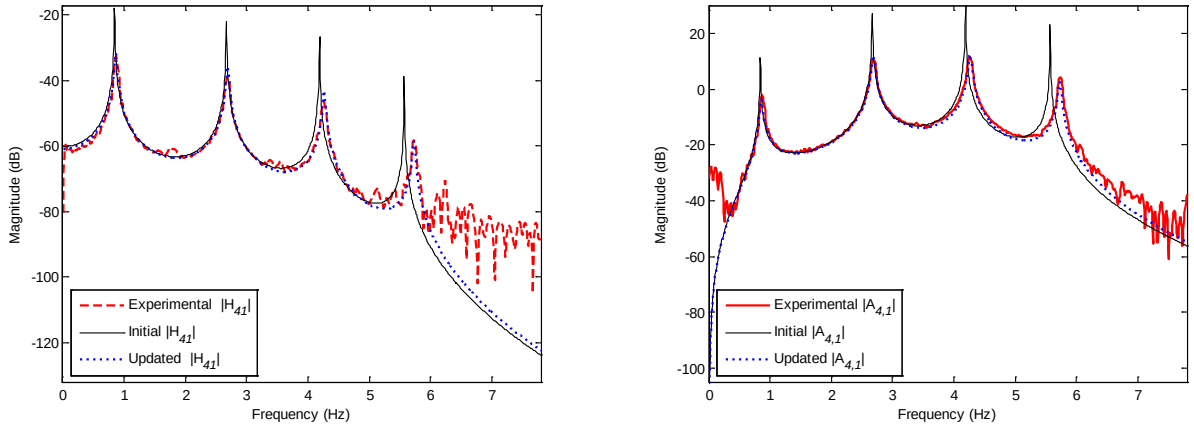

(a) Receptance $\mathbf{H}_{4,1}$ (b) Accelerance $\mathbf{A}_{4,1}$

Figure 4. Hammer test: comparison of the initial, the experimental and the updated FRFs (Rayleigh damping)

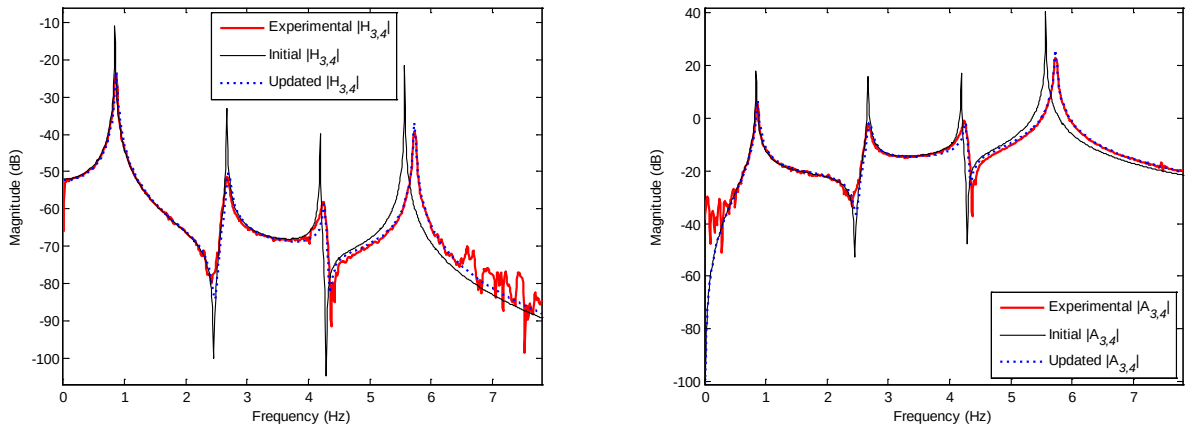

(a) Receptance $\mathbf{H}_{3,4}$ (b) Accelerance $\mathbf{A}_{3,4}$

Figure 5. Hammer test: comparison of the initial, the experimental and the updated FRFs (Caughey damping)

adopted as the ground excitation. After the test, FRF-based model updating is applied to the receptances and accelerances calculated using the response of every floor and the measured chirp excitation at the ground floor. Figure 6 shows the measured ground excitation time history. Figure 7 shows the measured acceleration and displacement response time history of the 1st floor.

Table 2 summarizes updating results from the shake table test. Receptances and accelerances are updated for both Rayleigh damping model and Caughey damping model. The largest RSD value of the updating variable is only 1.886%. In Rayleigh damping case, the values of updated a_0 from receptances and accelerances have a large difference. While in Caughey damping case, the damping ratio of every mode updated from receptances and accelerances is consistent. Therefore, Caughey damping model is assumed to be more suitable than Rayleigh damping model for this structure.

Figure 8 shows the updated FRF plots using Rayleigh damping model. Figure 8(a) compares the initial, the experimental and the updated receptance $\mathbf{H}_{2,\text{ground}}$. Figure 8 (b) shows the comparison for accelerance $\mathbf{A}_{2,\text{ground}}$. The peak areas for these updated FRF curves can match well with the peak areas of experimental FRF curves. The FDAC value in Figure 8 (a) is 0.990 and the FDAC value in Figure 8 (b) is 0.949. Figure 9 shows the updated FRF plots using Caughey damping model. Figure 9 (a) compares the initial, the experimental and the updated receptance $\mathbf{H}_{4,\text{ground}}$. Figure 9 (b) shows the comparison for accelerance $\mathbf{A}_{4,\text{ground}}$. The FDAC value in Figure 9 (a) is 0.991 and the FDAC value in Figure 9 (b) is 0.958. Same as the hammer test scenario, the overall FDAC values in Caughey damping case are larger than those in Rayleigh damping case.

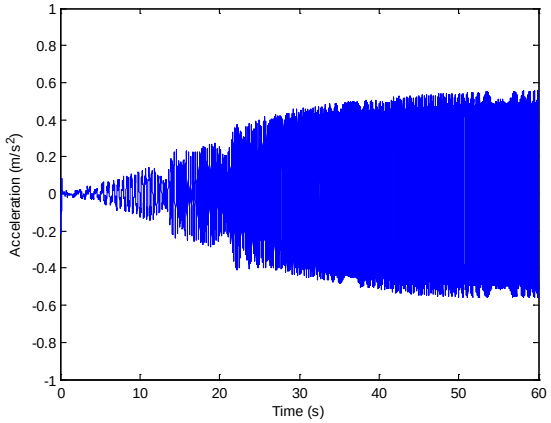

Figure 6. Ground acceleration time history

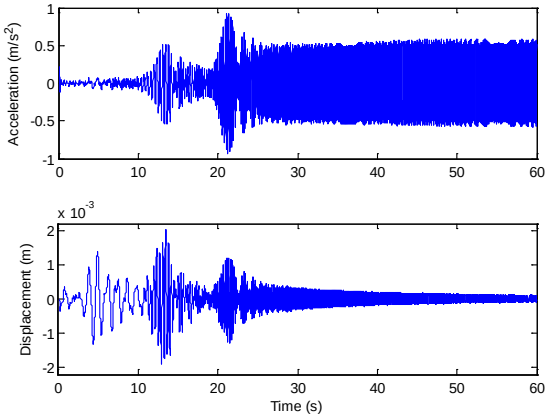

Figure 7. Responses time history of 1st floor

Table 2. Model updating results from ground excitation

Parameter		Initial	Rayleigh damping		Caughey damping		RSD (%)
			Updated (Receptance)	Updated (Accelerance)	Updated (Receptance)	Updated (Accelerance)	
Mass (kg)	m_1	4.64	5.155	5.146	5.155	5.155	0.092
	m_2	4.64	5.067	4.953	5.155	5.155	1.886
	m_3	4.64	4.949	4.949	4.949	4.949	0.000
	m_4	4.64	5.143	5.143	5.143	5.143	0.000
Stiffness (N/m)	k_1	1019	1066.005	1071.018	1049.846	1054.194	0.934
	k_2	1217	1271.367	1255.729	1289.074	1292.659	1.337
	k_3	1420	1363.619	1334.025	1392.786	1381.518	1.873
	k_4	2473	2712.432	2711.849	2696.013	2692.271	0.389
Damping	a_0 or ξ_1	0.01 / 0.01	0.2850	0.1530	0.0142	0.0142	-
	a_1 or ξ_2	10^{-6} / 0.01	0.0001	0.0001	0.0070	0.0070	-
	ξ_3	0.01	-	-	0.0056	0.0058	-
	ξ_4	0.01	-	-	0.0064	0.0081	-

Comparison between the updating results from hammer tests and the shake table test (Table 1 and Table 2) show that the mass and stiffness results are stable between the two tests. However, large differences are observed for damping results. As expected, it is shown that damping is much more challenging to characterize than mass and stiffness.

5. SUMMARY AND DISCUSSION

This research investigates the FRF-based FE model updating method. The method minimizes the difference between the experimental and analytical FRFs. The modal-decomposed form of analytical FRF is used in updating procedure. Experimental model updating is performed on a 4-story shear-frame laboratory structure. Two different types of FRFs (accelerance and receptance) with Rayleigh damping model and Caughey damping model are used to compare the updating results. Two test scenarios are studied: one is hammer test, and the other is shake table test. In order to get more FRF information at different locations, the displacement and acceleration of every floor of the structure are measured in all tests. The model updating results show that updating variables associated with mass and stiffness have better consistency from different test scenarios than the damping variables. In addition, Caughey damping case gives better performance in model

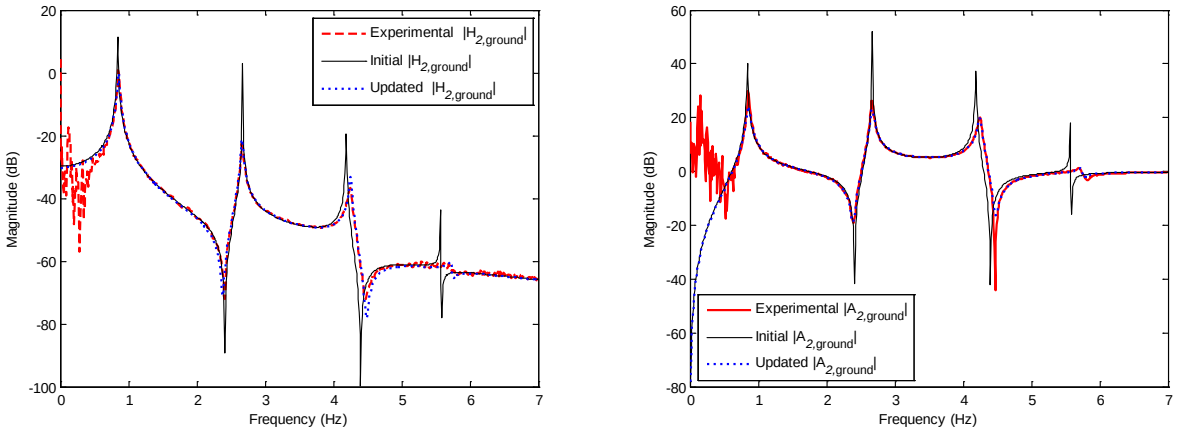

(a) Receptance $\mathbf{H}_{2,\text{ground}}$ (b) Accelerance $\mathbf{A}_{2,\text{ground}}$

Figure 8. Shake table test: comparison of the initial, the experimental and the updated FRFs (Rayleigh damping)

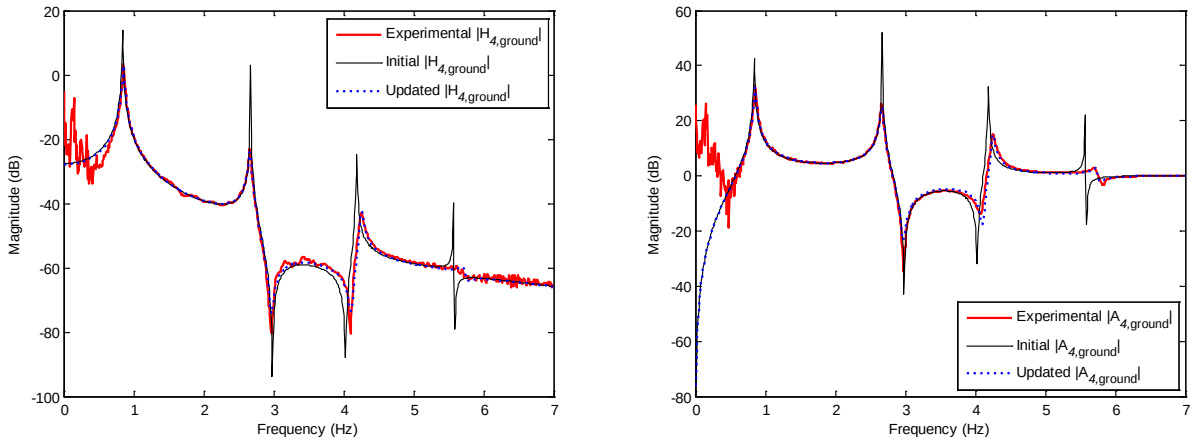

(a) Receptance $\mathbf{H}_{4,\text{ground}}$ (b) Accelerance $\mathbf{A}_{4,\text{ground}}$

Figure 9. Shake table test: comparison of the initial, the experimental and the updated FRFs (Caughey damping)

updating, but it can be more time-consuming for large FE models. In the future, more damping models will be studied for this structure, and the FRF-based FE model updating will be performed on more realistic structures.

ACKNOWLEDGEMENT

This research is partially supported by the National Science Foundation (CMMI-1150700) and the China Scholarship Council. The authors gratefully acknowledge the support. Any opinions, findings, and conclusions or recommendations expressed in this publication belong to those authors and do not necessarily reflect the view of the sponsors.

REFERENCES

[1] Friswell, M.I. and Mottershead, J.E., [Finite element model updating in structural dynamics], Kluwer Academic Publishers, Dordrecht & Boston (1995).
[2] Brownjohn, J.M.W. and Xia, P.Q., "Dynamic assessment of curved cable-stayed bridge by model updating," J. Struct. Engrg. 126(2), 252-260 (2000).
[3] Teughels, A., Maeck, J. and De Roeck, G., "A finite element model updating method using experimental modal parameters applied on a railway bridge," Proc. 7th Int. Conf. on Computer Aided Optimum Design of Structures 54, 97-106 (2001).
[4] Jaishi, B. and Ren, W.-X., "Structural finite element model updating using ambient vibration test results," J. Struct. Engrg. 131(4), 617-628 (2005).
[5] Abdalla, M.O., Grigoriadis, K.M. and Zimmerman, D.C., "Structural damage detection using linear matrix inequality methods," J. Vib. Acoust. 122(4), 448-455 (2000).
[6] Zhu, D., Dong, X. and Wang, Y., "A comparative study on modal-based finite element model updating approaches using noisy measurements," Proc. the 11th International Conference on Structural Safety & Reliability (ICOSSAR), (2013).
[7] Agbabian, M., Masri, S., Miller, R. and Caughey, T., "System Identification Approach to Detection of Structural Changes," J. Engrg. Mech. 117(2), 370-390 (1991).
[8] Cattarius, J. and Inman, D.J., "Time domain analysis for damage detection in smart structures," Mech. Syst. Signal Pr. 11(3), 409-423 (1997).

[9] Lin, R.M. and Ewins, D.J., "Analytical model improvement using frequency response functions," Mech. Syst. Signal Pr. 8(4), 437-458 (1994).
[10] Lin, R.M. and Zhu, J., "Model updating of damped structures using FRF data," Mech. Syst. Signal Pr. 20(8), 2200-2218 (2006).
[11] Arora, V., Singh, S.P. and Kundra, T.K., "Finite element model updating with damping identification," J. Sound Vib. 324(3–5), 1111-1123 (2009).
[12] Pradhan, S. and Modak, S.V., "Normal response function method for mass and stiffness matrix updating using complex FRFs," Mech. Syst. Signal Pr. 32, 232-250 (2012).
[13] Sipple, J.D. and Sanayei, M., "Finite element model updating using frequency response functions and numerical sensitivities," Struct. Health Monit. 21(5), 784-802 (2014).
[14] Caughey, T.K. and O'Kelly, M.E.J., "Classical normal modes in damped linear dynamic systems," J. Appl. Mech. 32(3), 583-588 (1965).
[15] Chopra, A.K., [Dynamics of structures: theory and applications to earthquake engineering], Prentice Hall Pubishers, Upper Saddle River (2001).
[16] Kane, M., Zhu, D., Hirose, M., Dong, X., Winter, B., Häckell, M., Lynch, J.P., Wang, Y. and Swartz, A., "Development of an extensible dual-core wireless sensing node for cyber-physical systems," Proc. SPIE 9061, (2014).
[17] Nefske, D.J. and Sung, S.H., "Correlation of a coarse-mesh finite element model using structural system identification and a frequency response assurance criterion," Proc. the 14th International Modal Analysis Conference 597-602 (1996).